

AuthFace: Towards Authentic Blind Face Restoration with Face-oriented Generative Diffusion Prior

Guoqiang Liang^{1,2} Qingnan Fan² Bingtao Fu² Jinwei Chen² Hong Gu² Lin Wang^{1,3}

¹AI Thrust, HKUST(GZ) ²VIVO, Hangzhou, China

³Dept. of Computer Science and Engineering, HKUST

liangskylake@foxmail.com fqnchina@gmail.com linwang@ust.hk

bingtaofu, jinwei.chen, guhong@vivo.com

Project Page: <https://github.com/EthanLiang99/AuthFace>

Abstract

Blind face restoration (BFR) is a fundamental and challenging problem in computer vision. To faithfully restore high-quality (HQ) photos from poor-quality ones, recent research endeavors predominantly rely on facial image priors from the powerful pretrained text-to-image (T2I) diffusion models. However, such priors often lead to the incorrect generation of non-facial features and insufficient facial details, thus rendering them less practical for real-world applications. In this paper, we propose a novel framework, namely **AuthFace** that achieves highly authentic face restoration results by exploring a face-oriented generative diffusion prior. To learn such a prior, we first collect a dataset of 1.5K high-quality images, with resolutions exceeding 8K, captured by professional photographers. Based on the dataset, we then introduce a novel face-oriented restoration-tuning pipeline that fine-tunes a pretrained T2I model. Identifying key criteria of quality-first and photography-guided annotation, we involve the retouching and reviewing process under the guidance of photographers for high-quality images that show rich facial features. The photography-guided annotation system fully explores the potential of these high-quality photographic images. In this way, the potent natural image priors from pretrained T2I diffusion models can be subtly harnessed, specifically enhancing their capability in facial detail restoration. Moreover, to minimize artifacts in critical facial areas, such as eyes and mouth, we propose a time-aware latent facial feature loss to learn the authentic face restoration process. Extensive experiments on the synthetic and real-world BFR datasets demonstrate the superiority of our approach. *Codes and datasets will be available upon acceptance.*

1 Introduction

Face images captured in natural settings often exhibit various forms of degradation, including compression, blur, and noise [49, 51]. Capturing high-quality (HQ) face images is crucial, as humans are highly sensitive to subtle facial details. Blind face restoration (BFR) aims to reconstruct HQ images from degraded inputs and has rapidly progressed in recent years due to significant research interest. However, BFR remains an ill-posed problem due to the unknown degradation and the loss of valuable information resulting from these complex conditions [68].

Sufficient prior information is critical for HQ reconstruction. Researchers have used geometric and reference priors from sources like [3, 5, 10, 18, 23, 26–28, 37, 41, 57, 61, 69] to guide face restoration. These priors, however, are limited by their sensitivity to degradation and inability to capture fine facial details. With advancements in generative models, such as StyleGAN [20] and VQVAE [36], recent works [4, 5, 45, 49, 50, 53, 56, 68] have leveraged pretrained networks to derive facial priors, achieving superior results compared to earlier methods. Nonetheless, these approaches still face

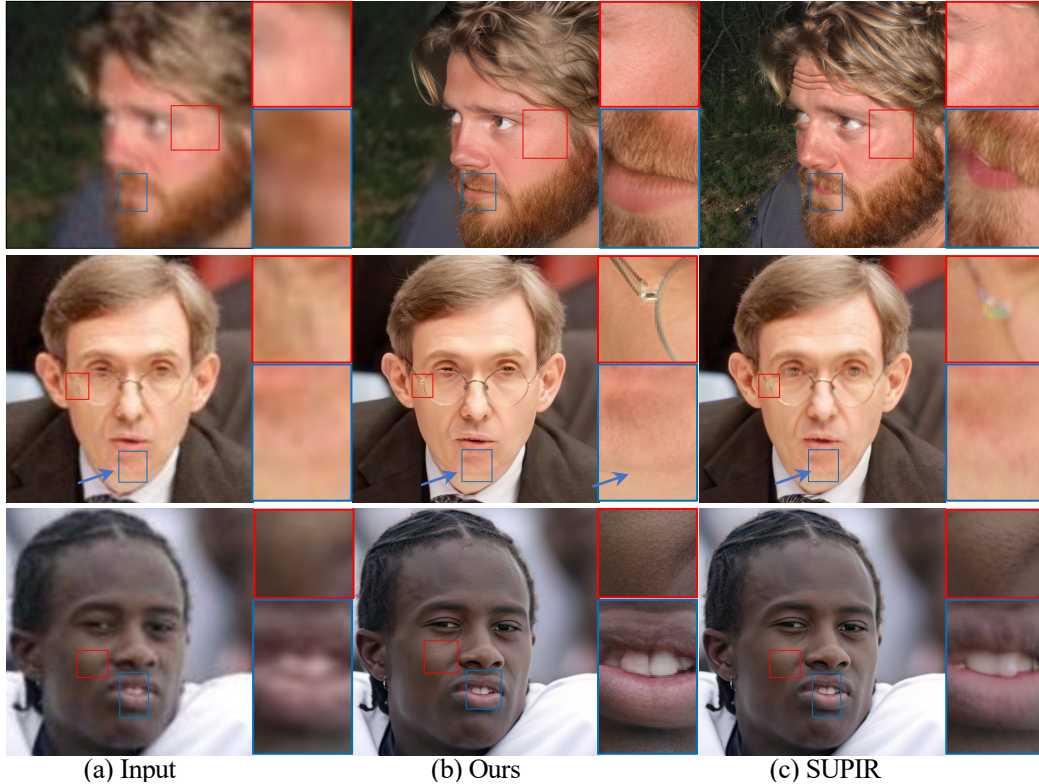


Figure 1: Compared with the results from a state-of-the-art (SOTA) method SUPIR [60] using StableDiffusion-XL (SDXL) [35] as prior, our approach excels in capturing and rendering intricate facial details. For instance, our result has a more distinct jawline (see blue arrow) in the 2nd row, effectively distinguishing the jaw from the neck. Zoom in for more details.

significant performance declines in handling unseen cases. Denoising diffusion probabilistic models (DDPMs) [16] have shown promise as an alternative to generative adversarial networks (GANs) [42] in image generation. Some approaches [51, 62] use pretrained DDPMs to diffuse and then denoise degraded inputs. However, their practical application is hindered by the loss of original identity and detailed facial features [33], with pretrained DDPMs also facing limitations in representational capacity.

The remarkable success of large-scale pretrained text-to-image (T2I) models [38, 39] has provided another promising prior. Many researchers explore the potential of StableDiffusion (SD) models [43] as the powerful prior in challenging low-level vision tasks, including real-world image super-resolution [29, 48, 54, 60] and BFR [6, 12]. Since the face details are often lost due to the degradation and down-sampling processes of VAE [38] in SD models, BFRffusion [6] and Diff-MAC [12] rely on the facial priors within SD models to recreate these details. However, being designed for general text-to-image tasks, SD models often fail to retain essential facial details, like skin texture (see Fig. 2 (b)). Therefore, these methods typically produce overly smooth images in the T2I task. Moreover, their extensive image priors can lead to the incorrect generation of non-facial features, resulting in artifacts, especially for images with ambiguous degradation. *These specific limitations – incorrect generation of non-facial features (blue box at 1st row of Fig. 1) and missing facial details (red box at 3rd row of Fig. 1)– severely limit the practical deployment of these models in real-world applications.*

To tackle these problems, we propose **Authface**, a novel BFR method with face-oriented generative diffusion prior, designed to restore highly authentic face images. The **highlight** of our Authface is that it brings a paradigm shift for BFR – with a two-stage training pipeline: 1) *Face-oriented Fine-tuning on Pretrained T2I Model*, and 2) *Highly Authentic Face Restoration*. The underlying premise for Stage I is that pretrained T2I models *e.g.*, SD models, can serve as effective generative diffusion priors for restoration tasks (Sec. 3.1). They can be customized for face-centric applications via fine-tuning while retaining their generation capabilities.



Figure 2: (a) A HQ face image with its paired tags generated through photography-guided image annotation. Specifically, we provide an additional photographic tag (blue box) beyond the semantic tags used in previous methods (gray box). (b) Qualitative comparison between StableDiffusion-XL (SDXL) [35] and our fine-tuned model, which is exclusively trained on the collected high-quality dataset, in the T2I task. Notably, SDXL tends to generate over-smooth skin even when given prompts specifying sharp details and sharp focus. Zoom in for more details.

In analyzing key factors for fine-tuning pretrained T2I models to meet human preferences for authentic facial images, we identify two key criteria as our face-oriented generative diffusion prior: 1) **Quality-first image collection**. Contrary to training T2I base models with large datasets like LAION-5B [40], the quality of the dataset, rather than its size, dictates the generation quality in the fine-tuning process. 2) **Photography-guided image annotation**. Fine-tuning the pretrained T2I models for HQ facial tasks requires more than just basic annotations like human accessories, especially for HQ face images with a pronounced stylistic orientation (see Fig. 2 (a)). In line with our established criteria, we collect a curated dataset of **1.5K** HQ face images – each enriched with detailed photographic annotations – to fine-tune the pretrained T2I models for the first stage. With the curated dataset, we are able to fine-tune the T2I models following their original optimization strategies, as illustrated in Fig. 3. With fine-tuning, the pretrained T2I model is required with the detailed facial prior, which can be demonstrated with the T2I task as shown in Fig. 2 (b). To achieve the goal of highly authentic face restoration in Stage II, we leverage the ControlNet [63] for training (Sec. 3.2). However, directly following the protocol of training ControlNet with the MSE loss tends to contribute to the loss of key facial details, such as eyes and mouths. To resolve this issue, we propose a **time-aware latent facial feature loss** to directly constrain the regions where humans are sensitive in the latent space. Our extensive experiments demonstrate the superior authentic detail generation performance on synthetic and real-world datasets.

In summary, our major contributions are three-fold: **I) Novel Research Direction**: Our work pioneers a new approach by enhancing the generative capabilities of pretrained T2I models for authentic face restoration, moving beyond traditional model design. **II) New Methodology**: Our AuthFace, a novel framework, enhances the detail handling of pretrained T2I models through a unique face-oriented restoration tuning pipeline. Our method significantly sharpens fine facial details and includes a time-aware latent facial feature loss, which effectively reduces artifacts in critical areas like the eyes and mouth. **III) New High-quality Dataset**: We have compiled a dataset of **1.5K** high-resolution images. We expect it can serve as a foundational and important resource to further advance the field of high-fidelity authentic face restoration.

2 Related Works

Prior-based Blind Face Restoration Blind face restoration (BFR) employs a variety of priors, classified into geometric, reference, and generative categories. Geometric priors, such as facial landmarks [3, 23], face parsing maps [5, 41, 57], facial component heatmaps [61], and 3D face shapes [18, 37, 69], provide crucial structural information for restoring degraded faces. Reference-based methods use images to deliver identity information, enhancing the fidelity of the restored faces [10, 26–28]. Moreover, some researchers have implemented generative facial priors, like StyleGAN [20], to refine facial details [4, 5, 49, 50, 56]. Another approach involves using pretrained Vector-Quantize codebooks that contain detailed facial information [45, 53, 68]. Given their remarkable performance in image generation, denoising diffusion probabilistic models [16] have become

increasingly popular in BFR. Notable examples, such as DiffFace [62], DR2 [51], and PGDiff [58], utilize denoising U-Nets pretrained on HQ face datasets to achieve face restoration at pixel level. Specifically, Zhao *et al.* [65] attempts to improve the authentic performance via feeding network with enhanced ground-truth images. Recently, large-scale pretrained text-to-image models like StableDiffusion (SD)[43] have been employed to address the BFR problem. DiffBIR [29] leverages SD priors for real-world image super-resolution and BFR by incorporating degraded input image information in the latent space. Specifically targeting BFR, BFRfusion [6] extracts multi-scale facial features in the latent space from low-quality face images. *However, achieving authentic BFR with pretrained T2I models in the latent space remains underexplored.*

Fine-Tuning Fine-tuning is widely used to align pretrained large language models (LLMs) with human preferences, improving their effectiveness [2]. This technique, successful in LLMs with small, HQ datasets [44, 67], has been adapted to text-to-image models to enhance text-image alignment [9, 24, 25]. For example, Emu [9] improves aesthetic alignment using fine-tuned HQ image-text pairs. Playground v2.5 [24] enhances human features using a quality-controlled dataset, and CosmicMan [25] generates superior human-centric content with large, refined datasets. *However, these methods often produce overly smooth images, which may not be ideal for BFR tasks where authentic and realistic images are essential.*

3 Methodology

The goal of our work is to achieve authentic face restoration by minimizing unrealistic outcomes and enhancing the rendition of human-preferred features. It is structured into two distinct stages: **1) Face-oriented Tuning on Pre-trained T2I Model.** We integrate supervised fine-tuning [34] and quality-tuning [9] strategies to refine StableDiffusion-XL (SDXL), enhancing it with detailed facial features as our face-oriented generative diffusion prior (Sec. 3.1); **2) Highly Authentic Face Restoration.** Utilizing the face-oriented generative diffusion prior, we implement ControlNet [63] to direct the restoration process based on the quality of input degradation (Sec.3.2). Moreover, we introduce a time-aware latent facial feature loss to improve key facial features during restoration (Sec.3.2).

3.1 Stage I: Face-oriented Fine-tuning on Pre-trained T2I Model

The face-oriented tuning procedure for a pre-trained T2I model consists of two main parts: 1) a quality-first dataset preparation process to obtain and filter HQ face images, and 2) photography-guided data annotation to move beyond basic labels that only convey semantic information.

Quality-first Image Collection. Training T2I models typically requires large datasets. However, akin to the significant performance improvements seen in large language models fine-tuned with just 1K HQ examples [67], it has been demonstrated that enhancing the aesthetic quality of generated results can be achieved with only a few thousand extremely HQ images [9]. This highlights that dataset quality is more important than size in the fine-tuning process. Inspired by this, we apply the quality-first principle to prepare our fine-tuning dataset.

Collecting HQ real-world face images is challenging due to privacy and copyright concerns, and existing datasets like FFHQ [19] suffer from issues such as JPEG degradation, blur, and Gaussian noise [65]. To overcome these challenges, we source extremely HQ face images from the professional photography website Unsplash [46], which offers a license supporting both commercial and non-commercial use. Although the collected images are captured and post-processed by professional photographers, not all images prominently feature faces. To address this, we implement a set of data filtering strategies to create an HQ, face-centric subset. These strategies include face detection to remove images without faces or with small faces, and image quality assessment to filter out images with excessive artifacts such as pepper noise. Also, we use face landmark detection to locate eyes and mouth, enabling us to follow the alignment process used in FFHQ [19, 21], better suited for the BFR task.

Recognizing the racial imbalance in our dataset (predominantly Caucasian and African descent), we collaborate with professional photographers to build an HQ dataset featuring individuals of Asian descent, using top-level studio settings. All facial images are manually filtered to ensure they present clear skin texture and hair details, resulting in a fine-tuning dataset of 1,500 extremely HQ images.

Photography-guided Image Annotation.

The quality of prompts is essential for both training [2] and fine-tuning [25] pretrained T2I models. For example, CosmicMan [25] fine-tunes SDXL for human-centric content generation by breaking human parsing maps into several parts to provide detailed annotations. However, for face-oriented tuning tasks, densely annotated images are less effective. After cropping and alignment, the semantic information in facial images is limited, often capturing only overall human attributes. This differs significantly from other tasks where densely packed semantic information is prevalent. For face-oriented tuning, capturing stylistic information beyond basic semantics is crucial. In portrait photography, this includes expressions, skin texture, makeup, and lighting, essential for authentic face restoration.

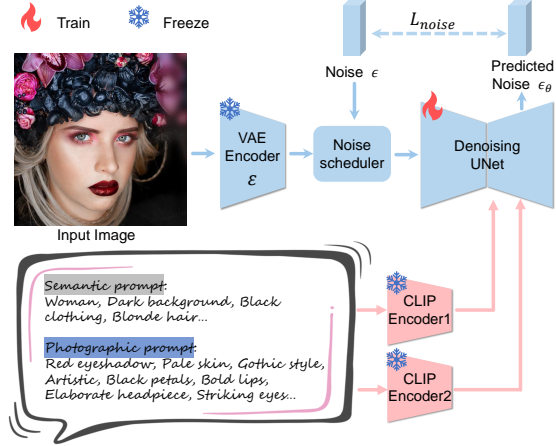


Figure 3: The framework of face-oriented tuning.

Therefore, we apply photography-guided data annotation to generate prompts for our fine-tuning dataset, especially given that our dataset consists of HQ portraits by professional photographers with strong stylistic tendencies. We follow previous methods [2, 25] to realize automatic captioning tasks with Vision-Language Models (VLMs). Specifically, we leverage the pretrained LLaVA-1.6 [30] as the automatic caption to generate a tag-style prompt to avoid redundant prepositions and adverbs [14]. Fig. 2 (a) illustrates some examples of photography-guided data annotation. Based on the dataset, we can fine-tune the pre-trained T2I model, SDXL, as shown in Fig. 3. Different from the training of SDXL, we fix the resolution of training images instead of multi-aspect training.

3.2 Stage II: Highly Authentic Face Restoration

Fig. 4 illustrates the structure of stage II. Given the fine-tuned SDXL model as our face-oriented generative diffusion prior, we need an adaptor that can control the fine-tuned SDXL to generate high-quality facial images based on its degraded input. With the successful application of ControlNet [63] in real-world image super-resolution [54, 60], we apply it as the controller for the BFR task.

The training of stage II is as follows. The latent representation of an HQ facial image is obtained by the encoder of a pretrained VAE, denoted as \mathbf{z}_0 . The diffusion process progressively introduces noise to \mathbf{z}_0 , resulting in a noisy latent \mathbf{z}_t , where t represents the randomly sampled diffusion step. The restoration is conditioned on the additional input \mathbf{c} , which is the degraded face image, guiding the generation process. For each diffusion step t , the noisy latent \mathbf{z}_t is processed together with the control condition \mathbf{c} , and null prompts [""]. We train the ControlNet by minimizing the L_2 loss between the predicted noise ϵ_θ and the added noise ϵ ($\epsilon \sim \mathcal{N}(0, I)$). The optimization objective is:

$$\mathcal{L}_{noise} = \mathbb{E}_{\mathbf{z}_0, t, \mathbf{c}, \epsilon \sim \mathcal{N}(0, I)} [\|\epsilon - \epsilon_\theta(\mathbf{z}_t, t, [""], \mathbf{c})\|_2^2]. \quad (1)$$

Specifically, we freeze the parameters of our fine-tuned SDXL model to preserve the enhanced facial priors and its original natural image priors. We initialize ControlNet with the encoder from our fine-tuned SDXL model while solely training ControlNet.

Time-aware Latent Facial Feature Loss. Reducing incorrect generation is crucial for authentic face restoration, as humans are sensitive to key facial features like eyes and mouths. However, the MSE loss (Eq. 1) used to train the ControlNet only provides a holistic constraint, where both the background and face of the degraded image equally influence optimization. Thanks to the spatially invariant features of the conditioning embedding module in ControlNet, the latent space retains spatial dimensions [1]. This allows for pixel-level constraints in the latent space.

To enhance key facial features, we propose a time-aware latent facial feature loss that provides additional constraints on the eyes and mouth. Inspired by GFP-GAN [49], we train separate facial feature discriminators to ensure these regions in the restored results match natural distributions. Unlike GFP-GAN, our method incorporates the diffusion and denoising process of DDPMs, *considering time as a variable*. Previous studies[1, 8, 48] show that during denoising, the generated results evolve from rough shapes to high-resolution images. Therefore, using shared model weights for various time

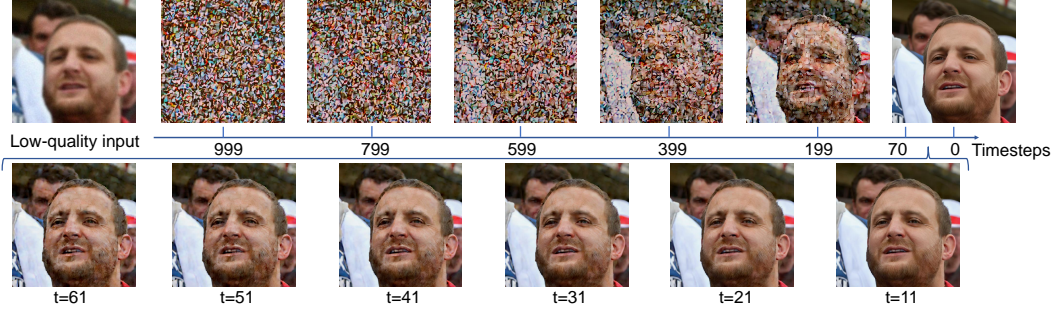


Figure 5: Visualization of the diffusion process at different steps. In the early steps ($t = 999 - 599$), the main content of the images is predominantly noise, with key facial features obscured. In the later steps ($t = 61 - 0$), the shapes of key facial features become fixed, with minimal changes.

Table 1: Quantitative results for blind face restoration on both synthetic and real-world datasets. The highest result is highlighted in **red** while the second highest result is highlighted in **blue**.

Datasets	Metrics	GFPGAN	PSFRGAN	CodeFormer	DR2	BFRffusion	SUPIR	Ours
CelebA	PSNR \uparrow	24.65	24.68	25.15	21.43	26.19	25.00	25.57
	SSIM \uparrow	0.6669	0.6322	0.6647	0.5943	0.6829	0.6487	0.6768
	LPIPS \downarrow	0.2308	0.2943	0.2269	0.3443	0.2272	0.2716	0.2143
	MANIQA \downarrow	0.5633	0.5103	0.5546	0.5397	0.5964	0.5233	0.6624
	MUSIQ \uparrow	73.91	73.32	75.56	70.42	71.90	72.92	75.76
	FID \downarrow	42.62	47.59	52.43	56.59	40.74	35.01	50.93
	CLIPQA \uparrow	0.6790	0.6310	0.6716	0.5770	0.6863	0.6103	0.7065
LFW	MANIQA \uparrow	0.5514	0.5176	0.5415	0.5326	0.5528	0.4768	0.6431
	MUSIQ \uparrow	73.58	73.60	75.49	71.04	69.86	69.90	75.87
	FID \downarrow	49.96	51.89	52.36	47.14	49.92	41.98	45.29
	CLIPQA \uparrow	0.6994	0.6471	0.6893	0.6069	0.6969	0.5931	0.7350
WebPhoto	MANIQA \uparrow	0.5351	0.4793	0.5241	0.4843	0.4721	0.4394	0.5860
	MUSIQ \uparrow	72.13	71.67	74.01	67.19	61.78	65.67	74.11
	FID \downarrow	87.35	88.45	83.19	107.86	84.29	73.44	90.04
	CLIPQA \uparrow	0.6888	0.6366	0.6922	0.5690	0.6308	0.5767	0.6964
WIDER	MANIQA \uparrow	0.5289	0.4925	0.5119	0.4989	0.4923	0.4522	0.5941
	MUSIQ \uparrow	72.80	71.50	73.40	67.18	61.87	67.19	74.59
	FID \downarrow	39.49	49.84	38.78	45.27	55.22	42.61	36.10
	CLIPQA \uparrow	0.7101	0.6482	0.6990	0.5943	0.6789	0.6093	0.7306

learning rate of $5e - 7$ during the finetuning process, where the batch size and the training iteration are set to 96 and 50k, respectively. We apply the same optimizer with the learning rate of $2e - 5$ with the batch size 48 for training ControlNet. All experiments are conducted on four NVIDIA L40s GPUs in the resolution of 1024×1024 for finetuning model and 512×512 for training ControlNet.

Training and Test Dataset: The training dataset for the fine-tuning process of our face-oriented model comprises **1.5K** high-quality face images, each enriched with detailed photographic annotations. For training our AuthFace network, we resize the FFHQ dataset [19] from a resolution of 1024×1024 to 512×512 . To form training pairs, we follow the settings, including degradation types and degrees, as outlined in previous methods [6, 49]. Following [58, 65, 68], we evaluate our method on a synthetic dataset, CelebA-Test [31], and three real-world datasets: LFW-Test [49], WebPhoto-Test [49], and WIDER-Test [68].

Metrics: To evaluate our method’s performance on the Celeb-A dataset with ground truth, we use PSNR [17], SSIM [52], and LPIPS [64]. Besides, we follow SUPIR [60] introducing non-reference image quality assessment metrics, MUSIQ [22], ManIQA [59], ClipIQA [47], and FID [15].

4.2 Comparison and Evaluation

We compare our method with SOTA BFR methods in three different categories: **(I)** GAN-based methods, including GFP-GAN [49] and PSFR-GAN [5]; **(II)** Codebook-based method, including CodeFormer [68]; **(III)** Diffusion-based methods, including DR2 [51] and BFRffusion [7]; Notably, we compare our method with SOTA IR method, SUPIR [60], which is also based on SDXL [35]. All methods are tested with official codes.

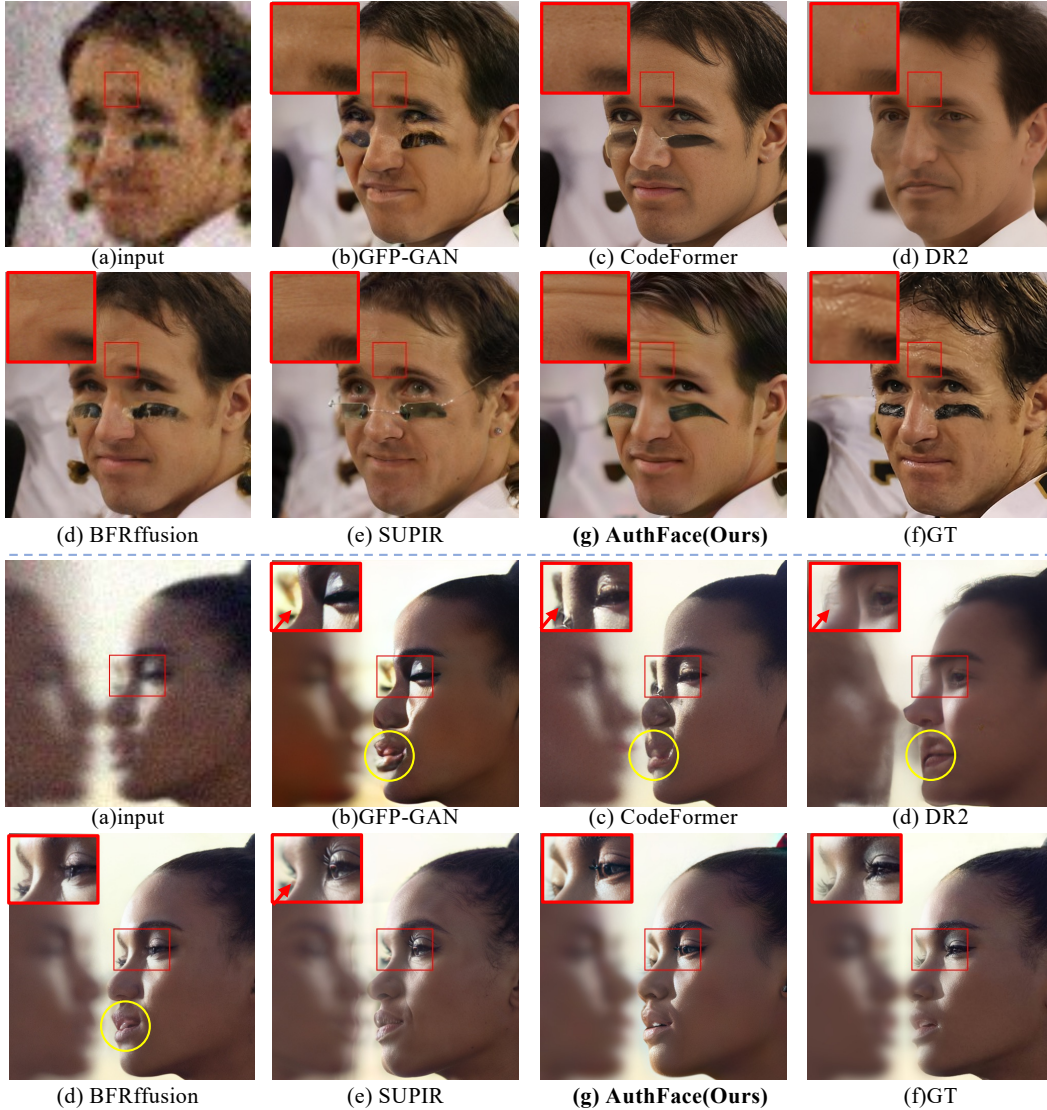


Figure 6: Qualitative results on CelebA-Test dataset. **Red box areas** in 1st row highlight the detailed skin texture and eyebrows achieved by our method. **Zoom in for details.**

Comparison on Synthetic Dataset: Quantitative results in Tab. 1 showcase our method’s superior performance on the CelebA-Test dataset, outperforming baselines in all non-reference image quality assessment metrics except FID. Notably, we achieve SOTA performance in terms of the LPIPS score. This marks a significant validation of our approach for the BFR task. Qualitatively, as depicted in Fig. 6, our AuthFace achieves authentic face restoration. Specifically, all methods except ours fail to recover the face paint in the first example, and our method results in the best hair detail. The second example involves recovering the side face, which is one of the most challenging cases in BFR [68]. GFP-GAN, CodeFormer, and BFRffusion fail to restore authentic mouth details (yellow circle), while the results from GFP-GAN, CodeFormer, DR2, and SUPIR lose the right eye (red box). Only our method produces realistic results in these key regions, with best details in the eyebrow and skin texture.

Comparison on Real-world Dataset: The robustness of our method is demonstrated by its SOTA performance in all metrics and real-world datasets, except for the FID score in the LFW-Test and WebPhoto-Test datasets, as shown in Tab. 1. Notably, the MANIQA score in the LFW-Test dataset exceeds the baselines by **0.09**. In the LFW-Test dataset, GFP-GAN, CodeFormer, and DR2 fail to reconstruct realistic results in the eye regions due to incorrect generation at the edges of glasses (see the red box in the first row of Fig. 7). In the second row of Fig. 7, our method outperforms others by accurately reconstructing both the upper and lower teeth without the artifacts around the

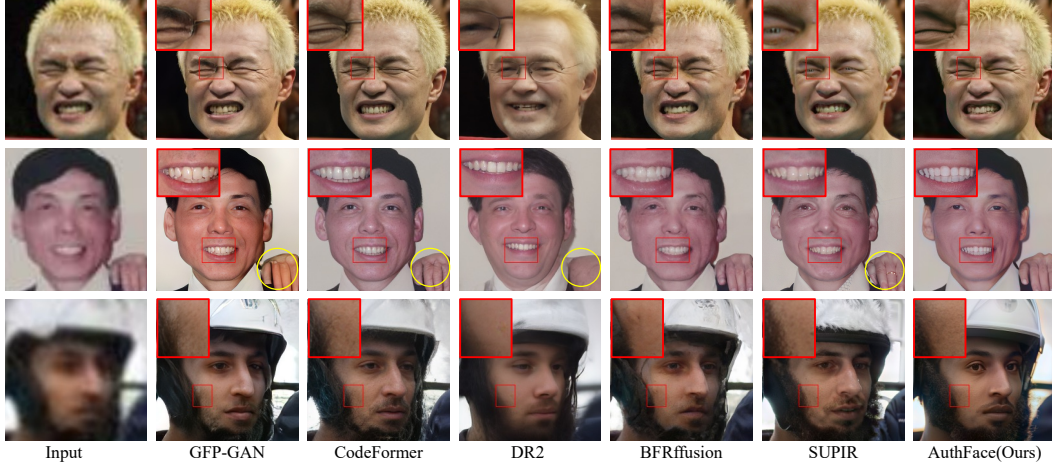


Figure 7: Qualitative results on real-world datasets. Results in 1st row are from LFW-Test dataset [49]. Results in 2nd row come from WebPhoto-Test dataset [49]. Results in 3rd row are from WIDER-Test dataset [68] including a zoomed-in view of the skin highlighted in red box areas. **Zoom in for details.** Table 2: Ablation studies of variant generative diffusion prior and time-aware latent facial feature loss. The highest result is highlighted in red while the second highest result is highlighted in blue.

Dataset	Exp.	Diffusion Prior		\mathcal{L}_{facial}		Metrics			
		SDXL	Ours	Const.	Time-aware	PSNR \uparrow	MANIQA \uparrow	MUSIQ \uparrow	CLIPQA \uparrow
CelebA	(a)	✓				24.39	0.5781	69.25	0.6465
	(b)		✓			25.59	0.5057	74.42	0.7088
	(c)		✓	✓		23.95	0.6449	73.66	0.6821
	(d)		✓		✓	25.57	0.6624	75.76	0.7065
WebPhoto	(a)	✓				-	0.5252	67.01	0.6276
	(b)		✓			-	0.5810	72.35	0.6833
	(c)		✓	✓		-	0.5767	68.52	0.6861
	(d)		✓		✓	-	0.5860	74.11	0.6964

hands, highlighted in a yellow circle. In the WebPhoto-Test dataset, our approach not only precisely reconstructs details such as helmets and goatees but also delivers the best skin texture, as showcased in the red box areas. *More visualization results are in the appendix and the supplmat.*

4.3 Ablation Study

We conduct ablation studies on CelebA-Test and WebPhoto-Test to assess the effectiveness of every part of our method.

Effectiveness of Face-oriented Fine-Tuning: We conducted an ablation study to evaluate the effectiveness of face-oriented tuning, as shown in Tab. 2 (a) and (b). In experiment (a), the original SDXL is used as the base model, and ControlNet is initialized with it. In experiment (b), the fine-tuned SDXL is used as the base model, and ControlNet is initialized with this fine-tuned version. Except for the MANIQA score on the CelebA-Test dataset, experiment (b) consistently outperforms experiment (a), highlighting the necessity of face-oriented tuning for the generative diffusion prior. Notably, in the WebPhoto-Test dataset, experiment (b) excels across all metrics, including CLIPQA (0.6833 vs. 0.6276), MUSIQ (72.35 vs. 67.01), and MANIQA (0.5810 vs. 0.5252). Experiment (b) enhances facial details such as eyebrows and skin texture (red box, first row in Fig. 8) and eyelashes (red box, second row). Additionally, it reduces errors in key facial features, resulting in clearer eyes (red box, first row) and better restoration of teeth (blue box, second row).

Effectiveness of Time-aware Latent Facial Feature Loss: To evaluate the effectiveness of the time-aware latent facial feature loss, we conducted experiments as shown in Tab. 2 (b), (c), and (d). Using constant weights for various time steps (experiment (c)) negatively impacts optimization, resulting in performance drops across most metrics, except for the MANIQA score on the CelebA-Test dataset compared to experiment (b). By focusing on steps when the major shapes of eyes and mouth emerge and assigning higher weights during these steps, our time-aware loss achieves the best performance

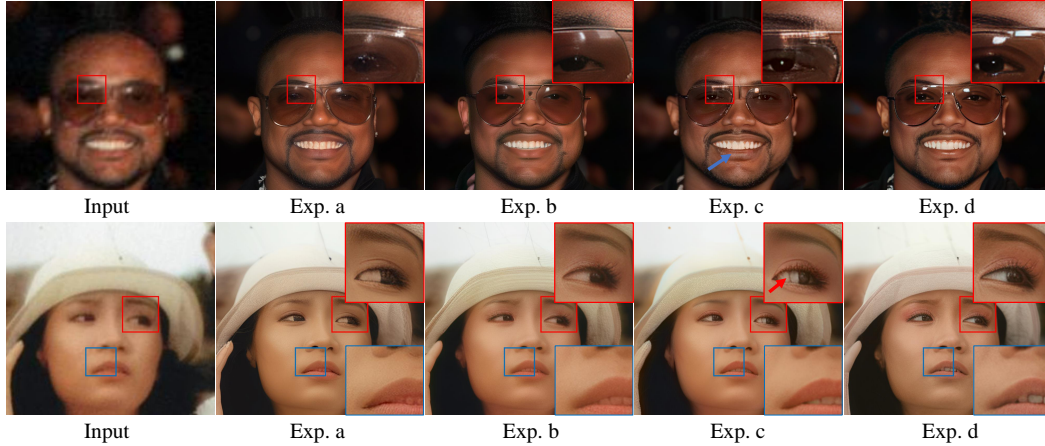


Figure 8: Visualization of ablation results. 1st row and 2nd row are the examples from CelebA-Test and WebPhoto-Test datasets, respectively. Please zoom in for more details.

on both synthetic and real-world datasets, except for the PSNR and CLIPQA scores on the CelebA dataset. As shown in Fig. 8, using latent space facial feature loss in experiments (c) and (d) improves the restoration of eyes and mouth (see the red box in the first row and the blue box in the second row). Notably, the time-aware strategy in experiment (d) not only reduces artifacts (as indicated by the blue and red arrows in Fig. 8) but also enhances details (e.g., the sharp edge of the glasses in the first row and the delicate skin texture and eyebrows in the second row).

5 Conclusion

This paper presented a new approach for achieving authentic face restoration by avoiding incorrect generations and enhancing facial details. Specifically, we proposed a face-oriented restoration-tuning paradigm to fine-tune the pretrained T2I model with high-quality face images, enabling the pretrained T2I model, SDXL, to develop a prior for facial details. Utilizing this face-oriented generative diffusion prior, we introduced AuthFace for the blind face restoration task, achieving authentic face restoration. Additionally, we introduced the time-aware latent facial feature loss to further improve the robustness of restoration in key facial features. Experimental results demonstrate the superiority and effectiveness of our method.

Limitation and Future Work: The process of collecting high-quality images requires significant human resources to filter out low-quality images. We plan to develop an aesthetic-oriented image quality assessment network to reduce labor costs.

References

- [1] Omri Avrahami, Ohad Fried, and Dani Lischinski. Blended latent diffusion. *ACM Transactions on Graphics (TOG)*, 42(4):1–11, 2023. 5
- [2] James Betker, Gabriel Goh, Li Jing, Tim Brooks, Jianfeng Wang, Linjie Li, Long Ouyang, Juntang Zhuang, Joyce Lee, Yufei Guo, et al. Improving image generation with better captions. *Computer Science*. <https://cdn.openai.com/papers/dall-e-3.pdf>, 2(3):8, 2023. 4, 5
- [3] Adrian Bulat and Georgios Tzimiropoulos. Super-fan: Integrated facial landmark localization and super-resolution of real-world low resolution faces in arbitrary poses with gans. In *Proceedings of the IEEE conference on computer vision and pattern recognition*, pages 109–117, 2018. 1, 3
- [4] Kelvin CK Chan, Xiangyu Xu, Xintao Wang, Jinwei Gu, and Chen Change Loy. Glean: Generative latent bank for image super-resolution and beyond. *IEEE Transactions on Pattern Analysis and Machine Intelligence*, 45(3):3154–3168, 2022. 1, 3
- [5] Chaofeng Chen, Xiaoming Li, Lingbo Yang, Xianhui Lin, Lei Zhang, and Kwan-Yee K Wong. Progressive semantic-aware style transformation for blind face restoration. In *Proceedings of the IEEE/CVF conference on computer vision and pattern recognition*, pages 11896–11905, 2021. 1, 3, 7
- [6] Xiaoxu Chen, Jingfan Tan, Tao Wang, Kaihao Zhang, Wenhan Luo, and Xiaochun Cao. Towards real-world blind face restoration with generative diffusion prior. *IEEE Transactions on Circuits and Systems for Video Technology*, 2024. 2, 4, 7
- [7] Xiaoxu Chen, Jingfan Tan, Tao Wang, Kaihao Zhang, Wenhan Luo, and Xiaochun Cao. Towards real-world blind face restoration with generative diffusion prior. *IEEE Transactions on Circuits and Systems for Video Technology*, 2024. 7
- [8] Jooyoung Choi, Jungbeom Lee, Chaehun Shin, Sungwon Kim, Hyunwoo Kim, and Sungroh Yoon. Perception prioritized training of diffusion models. In *Proceedings of the IEEE/CVF Conference on Computer Vision and Pattern Recognition*, pages 11472–11481, 2022. 5
- [9] Xiaoliang Dai, Ji Hou, Chih-Yao Ma, Sam Tsai, Jialiang Wang, Rui Wang, Peizhao Zhang, Simon Vandenhende, Xiaofang Wang, Abhimanyu Dubey, et al. Emu: Enhancing image generation models using photogenic needles in a haystack. *arXiv preprint arXiv:2309.15807*, 2023. 4
- [10] Berk Dogan, Shuhang Gu, and Radu Timofte. Exemplar guided face image super-resolution without facial landmarks. In *Proceedings of the IEEE/CVF conference on computer vision and pattern recognition workshops*, pages 0–0, 2019. 1, 3
- [11] Patrick Esser, Sumith Kulal, Andreas Blattmann, Rahim Entezari, Jonas Müller, Harry Saini, Yam Levi, Dominik Lorenz, Axel Sauer, Frederic Boesel, et al. Scaling rectified flow transformers for high-resolution image synthesis. *arXiv preprint arXiv:2403.03206*, 2024. 6
- [12] Nan Gao, Jia Li, Huaibo Huang, Zhi Zeng, Ke Shang, Shuwu Zhang, and Ran He. Diffmac: Diffusion manifold hallucination correction for high generalization blind face restoration. *arXiv preprint arXiv:2403.10098*, 2024. 2
- [13] Leon A Gatys, Alexander S Ecker, and Matthias Bethge. Image style transfer using convolutional neural networks. In *Proceedings of the IEEE conference on computer vision and pattern recognition*, pages 2414–2423, 2016. 6
- [14] Amir Hertz, Ron Mokady, Jay Tenenbaum, Kfir Aberman, Yael Pritch, and Daniel Cohen-Or. Prompt-to-prompt image editing with cross attention control. *arXiv preprint arXiv:2208.01626*, 2022. 5
- [15] Martin Heusel, Hubert Ramsauer, Thomas Unterthiner, Bernhard Nessler, and Sepp Hochreiter. Gans trained by a two time-scale update rule converge to a local nash equilibrium. *Advances in neural information processing systems*, 30, 2017. 7
- [16] Jonathan Ho, Ajay Jain, and Pieter Abbeel. Denoising diffusion probabilistic models. *Advances in neural information processing systems*, 33:6840–6851, 2020. 2, 3
- [17] Alain Hore and Djemel Ziou. Image quality metrics: Psnr vs. ssim. In *2010 20th international conference on pattern recognition*, pages 2366–2369. IEEE, 2010. 7
- [18] Xiaobin Hu, Wenqi Ren, John LaMaster, Xiaochun Cao, Xiaoming Li, Zechao Li, Bjoern Menze, and Wei Liu. Face super-resolution guided by 3d facial priors. In *Computer Vision–ECCV 2020: 16th European Conference, Glasgow, UK, August 23–28, 2020, Proceedings, Part IV 16*, pages 763–780. Springer, 2020. 1, 3

- [19] Tero Karras, Samuli Laine, and Timo Aila. A style-based generator architecture for generative adversarial networks. In *Proceedings of the IEEE/CVF conference on computer vision and pattern recognition*, pages 4401–4410, 2019. 4, 7, 15
- [20] Tero Karras, Samuli Laine, Miika Aittala, Janne Hellsten, Jaakko Lehtinen, and Timo Aila. Analyzing and improving the image quality of stylegan. In *Proceedings of the IEEE/CVF conference on computer vision and pattern recognition*, pages 8110–8119, 2020. 1, 3
- [21] Vahid Kazemi and Josephine Sullivan. One millisecond face alignment with an ensemble of regression trees. In *Proceedings of the IEEE conference on computer vision and pattern recognition*, pages 1867–1874, 2014. 4
- [22] Junjie Ke, Qifei Wang, Yilin Wang, Peyman Milanfar, and Feng Yang. Musiq: Multi-scale image quality transformer. In *Proceedings of the IEEE/CVF international conference on computer vision*, pages 5148–5157, 2021. 7
- [23] Deokyun Kim, Minseon Kim, Gihyun Kwon, and Dae-Shik Kim. Progressive face super-resolution via attention to facial landmark. *arXiv preprint arXiv:1908.08239*, 2019. 1, 3
- [24] Daiqing Li, Aleks Kamko, Ehsan Akhgari, Ali Sabet, Linmiao Xu, and Suhail Doshi. Playground v2. 5: Three insights towards enhancing aesthetic quality in text-to-image generation. *arXiv preprint arXiv:2402.17245*, 2024. 4
- [25] Shikai Li, Jianglin Fu, Kaiyuan Liu, Wentao Wang, Kwan-Yee Lin, and Wayne Wu. Cosmicman: A text-to-image foundation model for humans. *arXiv preprint arXiv:2404.01294*, 2024. 4, 5
- [26] Xiaoming Li, Chaofeng Chen, Shangchen Zhou, Xianhui Lin, Wangmeng Zuo, and Lei Zhang. Blind face restoration via deep multi-scale component dictionaries. In *European conference on computer vision*, pages 399–415. Springer, 2020. 1, 3
- [27] Xiaoming Li, Wenyu Li, Dongwei Ren, Hongzhi Zhang, Meng Wang, and Wangmeng Zuo. Enhanced blind face restoration with multi-exemplar images and adaptive spatial feature fusion. In *Proceedings of the IEEE/CVF Conference on Computer Vision and Pattern Recognition*, pages 2706–2715, 2020.
- [28] Xiaoming Li, Ming Liu, Yuting Ye, Wangmeng Zuo, Liang Lin, and Ruigang Yang. Learning warped guidance for blind face restoration. In *Proceedings of the European conference on computer vision (ECCV)*, pages 272–289, 2018. 1, 3
- [29] Xinqi Lin, Jingwen He, Ziyang Chen, Zhaoyang Lyu, Bo Dai, Fanghua Yu, Wanli Ouyang, Yu Qiao, and Chao Dong. Diffbir: Towards blind image restoration with generative diffusion prior, 2024. 2, 4
- [30] Haotian Liu, Chunyuan Li, Qingyang Wu, and Yong Jae Lee. Visual instruction tuning. *Advances in neural information processing systems*, 36, 2024. 5
- [31] Ziwei Liu, Ping Luo, Xiaogang Wang, and Xiaoou Tang. Deep learning face attributes in the wild. In *Proceedings of the IEEE international conference on computer vision*, pages 3730–3738, 2015. 7
- [32] Ilya Loshchilov and Frank Hutter. Decoupled weight decay regularization. *arXiv preprint arXiv:1711.05101*, 2017. 6
- [33] Yunqi Miao, Jiankang Deng, and Jungong Han. Waveface: Authentic face restoration with efficient frequency recovery. *arXiv preprint arXiv:2403.12760*, 2024. 2
- [34] Long Ouyang, Jeffrey Wu, Xu Jiang, Diogo Almeida, Carroll Wainwright, Pamela Mishkin, Chong Zhang, Sandhini Agarwal, Katarina Slama, Alex Ray, et al. Training language models to follow instructions with human feedback. *Advances in neural information processing systems*, 35:27730–27744, 2022. 4
- [35] Dustin Podell, Zion English, Kyle Lacey, Andreas Blattmann, Tim Dockhorn, Jonas Müller, Joe Penna, and Robin Rombach. Sdxl: Improving latent diffusion models for high-resolution image synthesis. *arXiv preprint arXiv:2307.01952*, 2023. 2, 3, 6, 7
- [36] Ali Razavi, Aaron Van den Oord, and Oriol Vinyals. Generating diverse high-fidelity images with vq-vae-2. *Advances in neural information processing systems*, 32, 2019. 1
- [37] Wenqi Ren, Jiaolong Yang, Senyou Deng, David Wipf, Xiaochun Cao, and Xin Tong. Face video deblurring using 3d facial priors. In *Proceedings of the IEEE/CVF international conference on computer vision*, pages 9388–9397, 2019. 1, 3

- [38] Robin Rombach, Andreas Blattmann, Dominik Lorenz, Patrick Esser, and Björn Ommer. High-resolution image synthesis with latent diffusion models. In *Proceedings of the IEEE/CVF conference on computer vision and pattern recognition*, pages 10684–10695, 2022. 2
- [39] Chitwan Saharia, William Chan, Saurabh Saxena, Lala Li, Jay Whang, Emily L Denton, Kamyar Ghasemipour, Raphael Gontijo Lopes, Burcu Karagol Ayan, Tim Salimans, et al. Photorealistic text-to-image diffusion models with deep language understanding. *Advances in neural information processing systems*, 35:36479–36494, 2022. 2
- [40] Christoph Schuhmann, Romain Beaumont, Richard Vencu, Cade Gordon, Ross Wightman, Mehdi Cherti, Theo Coombes, Aarush Katta, Clayton Mullis, Mitchell Wortsman, et al. Laion-5b: An open large-scale dataset for training next generation image-text models. *Advances in Neural Information Processing Systems*, 35:25278–25294, 2022. 3
- [41] Ziyi Shen, Wei-Sheng Lai, Tingfa Xu, Jan Kautz, and Ming-Hsuan Yang. Deep semantic face deblurring. In *Proceedings of the IEEE conference on computer vision and pattern recognition*, pages 8260–8269, 2018. 1, 3
- [42] Jiaming Song, Chenlin Meng, and Stefano Ermon. Denoising diffusion implicit models. *arXiv preprint arXiv:2010.02502*, 2020. 2, 6
- [43] Stability.ai. Stable diffusion 2. <https://stability.ai/stable-diffusion-2>, 2024. Accessed: 2024-05-15. 2, 4
- [44] Hugo Touvron, Thibaut Lavril, Gautier Izacard, Xavier Martinet, Marie-Anne Lachaux, Timothée Lacroix, Baptiste Rozière, Naman Goyal, Eric Hambro, Faisal Azhar, et al. Llama: Open and efficient foundation language models. *arXiv preprint arXiv:2302.13971*, 2023. 4
- [45] Yu-Ju Tsai, Yu-Lun Liu, Lu Qi, Kelvin CK Chan, and Ming-Hsuan Yang. Dual associated encoder for face restoration. *arXiv preprint arXiv:2308.07314*, 2023. 1, 3
- [46] Unsplash. Unsplash application programming interface (api). Unsplash, 2023. Accessed: 2023-11-18. 4
- [47] Jianyi Wang, Kelvin CK Chan, and Chen Change Loy. Exploring clip for assessing the look and feel of images. In *Proceedings of the AAAI Conference on Artificial Intelligence*, volume 37, pages 2555–2563, 2023. 7
- [48] Jianyi Wang, Zongsheng Yue, Shangchen Zhou, Kelvin CK Chan, and Chen Change Loy. Exploiting diffusion prior for real-world image super-resolution. In *arXiv preprint arXiv:2305.07015*, 2023. 2, 5
- [49] Xintao Wang, Yu Li, Honglun Zhang, and Ying Shan. Towards real-world blind face restoration with generative facial prior. In *The IEEE Conference on Computer Vision and Pattern Recognition (CVPR)*, 2021. 1, 3, 5, 7, 9
- [50] Yinhuai Wang, Yujie Hu, and Jian Zhang. Panini-net: Gan prior based degradation-aware feature interpolation for face restoration. In *Proceedings of the AAAI Conference on Artificial Intelligence*, volume 36, pages 2576–2584, 2022. 1, 3
- [51] Zhixin Wang, Ziyang Zhang, Xiaoyun Zhang, Huangjie Zheng, Mingyuan Zhou, Ya Zhang, and Yanfeng Wang. Dr2: Diffusion-based robust degradation remover for blind face restoration. In *Proceedings of the IEEE/CVF Conference on Computer Vision and Pattern Recognition*, pages 1704–1713, 2023. 1, 2, 4, 7
- [52] Zhou Wang, Alan C Bovik, Hamid R Sheikh, and Eero P Simoncelli. Image quality assessment: from error visibility to structural similarity. *IEEE transactions on image processing*, 13(4):600–612, 2004. 7
- [53] Zhouxia Wang, Jiawei Zhang, Runjian Chen, Wenping Wang, and Ping Luo. Restoreformer: High-quality blind face restoration from undegraded key-value pairs. In *Proceedings of the IEEE/CVF conference on computer vision and pattern recognition*, pages 17512–17521, 2022. 1, 3
- [54] Rongyuan Wu, Tao Yang, Lingchen Sun, Zhengqiang Zhang, Shuai Li, and Lei Zhang. Seesr: Towards semantics-aware real-world image super-resolution. *arXiv preprint arXiv:2311.16518*, 2023. 2, 5
- [55] Xiaoshi Wu, Yiming Hao, Keqiang Sun, Yixiong Chen, Feng Zhu, Rui Zhao, and Hongsheng Li. Human preference score v2: A solid benchmark for evaluating human preferences of text-to-image synthesis. *arXiv preprint arXiv:2306.09341*, 2023. 15, 17
- [56] Chengxing Xie, Qian Ning, Weisheng Dong, and Guangming Shi. Tfrgan: Leveraging text information for blind face restoration with extreme degradation. In *Proceedings of the IEEE/CVF conference on computer vision and pattern recognition*, pages 2534–2544, 2023. 1, 3

- [57] Lingbo Yang, Shanshe Wang, Siwei Ma, Wen Gao, Chang Liu, Pan Wang, and Peiran Ren. Hifacegan: Face renovation via collaborative suppression and replenishment. In *Proceedings of the 28th ACM international conference on multimedia*, pages 1551–1560, 2020. 1, 3
- [58] Peiqing Yang, Shangchen Zhou, Qingyi Tao, and Chen Change Loy. Pgdiff: Guiding diffusion models for versatile face restoration via partial guidance. *Advances in Neural Information Processing Systems*, 36, 2024. 4, 7
- [59] Sidi Yang, Tianhe Wu, Shuwei Shi, Shanshan Lao, Yuan Gong, Mingdeng Cao, Jiahao Wang, and Yujiu Yang. Maniqa: Multi-dimension attention network for no-reference image quality assessment. In *Proceedings of the IEEE/CVF Conference on Computer Vision and Pattern Recognition*, pages 1191–1200, 2022. 7
- [60] Fanghua Yu, Jinjin Gu, Zheyuan Li, Jinfan Hu, Xiangtao Kong, Xintao Wang, Jingwen He, Yu Qiao, and Chao Dong. Scaling up to excellence: Practicing model scaling for photo-realistic image restoration in the wild. In *Proceedings of the IEEE/CVF Conference on Computer Vision and Pattern Recognition*, pages 25669–25680, 2024. 2, 5, 7
- [61] Xin Yu, Basura Fernando, Bernard Ghanem, Fatih Porikli, and Richard Hartley. Face super-resolution guided by facial component heatmaps. In *Proceedings of the European conference on computer vision (ECCV)*, pages 217–233, 2018. 1, 3
- [62] Zongsheng Yue and Chen Change Loy. Difface: Blind face restoration with diffused error contraction. *arXiv preprint arXiv:2212.06512*, 2022. 2, 4
- [63] Lvmin Zhang, Anyi Rao, and Maneesh Agrawala. Adding conditional control to text-to-image diffusion models. In *Proceedings of the IEEE/CVF International Conference on Computer Vision*, pages 3836–3847, 2023. 3, 4, 5
- [64] Richard Zhang, Phillip Isola, Alexei A Efros, Eli Shechtman, and Oliver Wang. The unreasonable effectiveness of deep features as a perceptual metric. In *Proceedings of the IEEE conference on computer vision and pattern recognition*, pages 586–595, 2018. 7
- [65] Yang Zhao, Tingbo Hou, Yu-Chuan Su, Xuhui Jia, Yandong Li, and Matthias Grundmann. Towards authentic face restoration with iterative diffusion models and beyond. In *Proceedings of the IEEE/CVF International Conference on Computer Vision*, pages 7312–7322, 2023. 4, 7, 15
- [66] Yinglin Zheng, Hao Yang, Ting Zhang, Jianmin Bao, Dongdong Chen, Yangyu Huang, Lu Yuan, Dong Chen, Ming Zeng, and Fang Wen. General facial representation learning in a visual-linguistic manner. *arXiv preprint arXiv:2112.03109*, 2021. 6
- [67] Chunting Zhou, Pengfei Liu, Puxin Xu, Srinivasan Iyer, Jiao Sun, Yuning Mao, Xuezhe Ma, Avia Efrat, Ping Yu, Lili Yu, et al. Lima: Less is more for alignment. *Advances in Neural Information Processing Systems*, 36, 2024. 4
- [68] Shangchen Zhou, Kelvin C.K. Chan, Chongyi Li, and Chen Change Loy. Towards robust blind face restoration with codebook lookup transformer. In *NeurIPS*, 2022. 1, 3, 7, 8, 9
- [69] Feida Zhu, Junwei Zhu, Wenqing Chu, Xinyi Zhang, Xiaozhong Ji, Chengjie Wang, and Ying Tai. Blind face restoration via integrating face shape and generative priors. In *Proceedings of the IEEE/CVF conference on computer vision and pattern recognition*, pages 7662–7671, 2022. 1, 3

A Details of Face-oriented Tuning Datasets

Existing datasets like FFHQ [19] suffer from issues such as JPEG degradation, blur, and Gaussian noise [65]. We have compiled a collection of 1,500 high-quality images, exceeding resolutions of 8K, captured by professional photographers. These improvements address the quality limitations of traditional datasets, with examples showcased in Fig. 9 and Fig. 10.

We detail our dataset collection and annotation process in Fig. 11, which depicts the entire pipeline, including data collection, reviewing, and tagging. Apart from sourcing from Unsplash, we collaborate with professional photographers to collect studio-based images of Asian descent. These professionals also retouch each image to enhance skin texture while removing blemishes. All images undergo manual screening to ensure they are neither over-smoothed nor contain pepper noise, preserving detailed facial features.



Figure 9: Example of FFHQ datasets with noticeable blur and noise. Zoom in for more details.

B More ablation studies

Effectiveness of Face-oriented Fine-Tuning: To demonstrate the effectiveness of face-oriented fine-tuning, we conduct additional experiments on the task of text-to-image and provide more qualitative results on LFW-Test for the task of blind face restoration.

First, to underscore the value of our photography-guided annotation, we conducted ablation studies under three settings: (a) using the pretrained SDXL; (b) fine-tuning the SDXL with only semantic tags; and (c) fine-tuning with both semantic and our proposed photography-guided tags. We evaluated authenticity with FID and Human Preference Score v2 (Hpsv2) [55] and through a user study with 20 participants who assessed images from 10 prompts. According to Tab. 3, setting (c) not only scored the highest on FID and Hpsv2 but also received the best average ranking, indicating that users consistently preferred images produced by models fine-tuned with both semantic and our proposed photography-guided tags. Besides, Fig. 12 demonstrates that our face-oriented fine-tuning successfully equips SDXL with dedicated facial details.

To further evaluate the effectiveness of face-oriented fine-tuning We provide more qualitative results on LFW-Test as shown in Fig. 13. In experiment (a), the original SDXL is used as the base model,



Figure 10: Example of our HQ datasets with details of skin texture. Zoom in for more details.

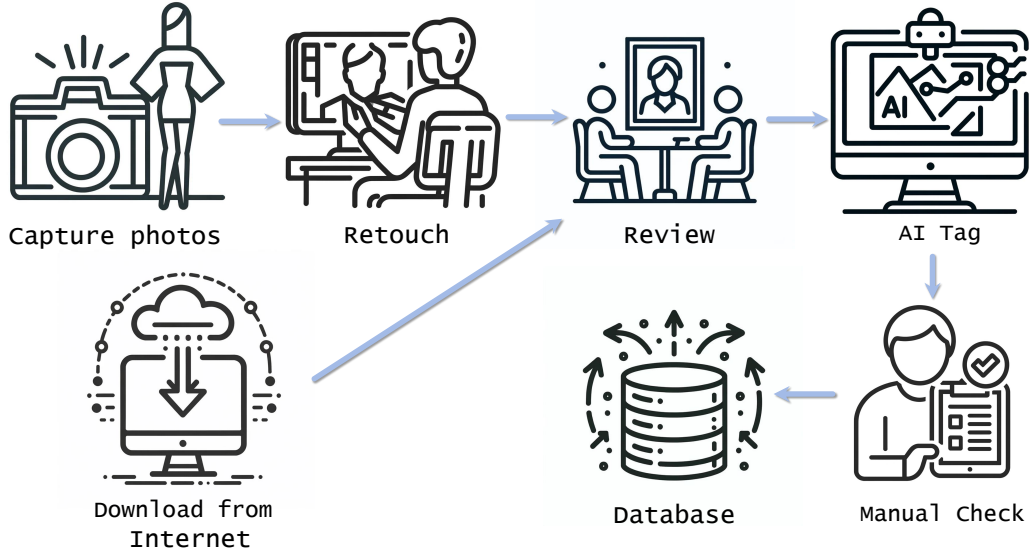


Figure 11: Illustration of collecting high-quality datasets for face-oriented fine-tuning.

and ControlNet is initialized with it. In experiment (b), the fine-tuned SDXL is used as the base model, and ControlNet is initialized with this fine-tuned version. Notably, the results of Exp. b has the best visual experience enjoying authentic facial details, such as the dedicated skin texture and hair, which demonstrates the importance of face-oriented fine-tuning.

Different hyper meter of time-aware latent facial feature loss: Through our face detection experiments, we identified that the timestep where the average confidence score reaches 0.5 is 0.32 (normalized) in the FFHQ dataset. We designated this timestep as the most critical, assigning it the highest weight. Therefore, we set the m as -0.5 and s as 1.0, where Eq. 3 in the main paper peaks at $t=0.37$. We conduct an ablation study on these hyperparameters m and s as detailed in Tab. 4 and we



Figure 12: More qualitative comparison of the text-to-image task between (a) using the pretrained SDXL; (b) fine-tuning the SDXL with only semantic tags; and (c) fine-tuning with both semantic and our proposed photography-guided tags.

Table 3: Ablation studies of variant tags used in fine-tuning. The highest result is highlighted in **red**, while the second highest result is are **blue** for clarity.

Exp	FID ↓	Hpsv2 [55] ↑	User study rank ↓
(a)	95.13	0.2637	2.53
(b)	62.90	0.2712	2.17
(c)	51.09	0.2903	1.33

also provide Fig. 14 showing the weight distributions of different hypermeter. This study confirms that our chosen settings yield the best outcomes, thus validating the robustness of our experimental approach.

C User Study:

We implemented an AB-test with 20 participants using 20 facial images from our datasets to gauge human perception of our method compared to six baselines. Participants were shown two images, labeled A and B, and asked to choose from three responses: "A is better," "B is better," or "Both are equally good," with image positions randomized. As detailed in Tab. 5, our method was preferred, indicating it produces results that are both more authentic and visually appealing.

Table 4: Ablation studies of variant generative diffusion prior and time-aware latent facial feature loss. The highest result is highlighted in **red** while the second highest result is highlighted in **blue**.

Dataset	Exp.	Location parameter m	Metrics			
			PSNR↑	MANIQA↑	MUSIQ↑	CLIPQA↑
CelebA	(a)	m = -0.5	25.57	0.6624	75.76	0.7065
	(b)	m = 0.0	25.40	0.6399	74.92	0.6786
	(c)	m = 0.5	25.37	0.6462	74.67	0.6882
	(d)	s = 0.5	25.42	0.6440	74.72	0.6794
WebPhoto	(a)	m = -0.5	-	0.5860	74.11	0.6964
	(b)	m = 0.0	-	0.5760	73.51	0.6657
	(c)	m = 0.5	-	0.5829	73.40	0.6755
	(d)	s = 0.5	-	0.5756	73.06	0.6686



Figure 13: Visualization of ablation results on LFW-Test dataset. Zoom in for more details.

Table 5: Results of user study. "Ours" is the percentage that our result is preferred, "Others" is the percentage that some other method is preferred, "Same" is the percentage that the users have no preference.

Methods	Others	Same	Ours
GFPGAN	26.75%	2.5%	70.75%
PSFRGAN	7.5%	0.75%	91.75%
CodeFormer	23.5%	1.25%	75.25%
DR2	10.5%	0.5%	89%
BFRffusion	25.25%	2%	72.75%
SUPIR	22.5%	1%	76.5%

D Running time

We evaluated our method’s runtime on a single NVIDIA L40s GPU, as detailed in Tab. 6. Notably, although both our method and SUPIR utilize SDXL, SUPIR demands significantly more time due to its initial enhancement phase and the use of LLaVA for text prompts. This supports our decision to omit details prompts in stage 2.

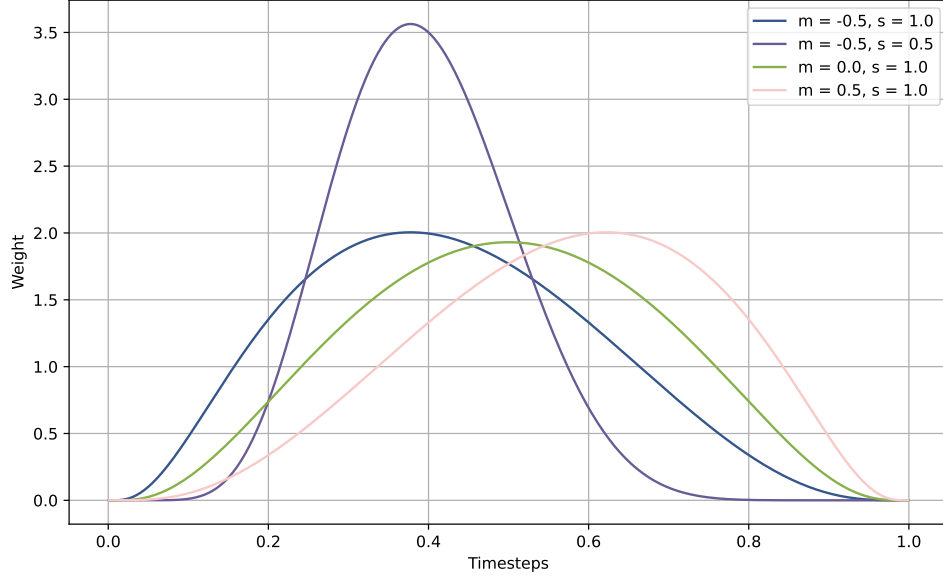


Figure 14: The weight distributions of different hyper meters of time-aware latent facial feature loss.

Table 6: Running time of different networks. Please note that all methods are evaluated in 512×512 input images, while DR2 reconstructs high-quality face images at 256×256 and upscale to 512×512 with an enchantment module according to its official setting.

Method	PSFRGAN	GFP-GAN	CodeFormer	DR2	BFRffusion	SUPIR	Ours
Time (s)	0.06	0.17	0.01	0.49	2.89	10.36	5.25

E More visualization results

In this section, we provide more visual comparisons with state-of-the-art methods in CelebA-Test, LFT-Test, WebPhoto-Test, and WIDER-Test datasets as shown in Fig. 15 and Fig. 16.

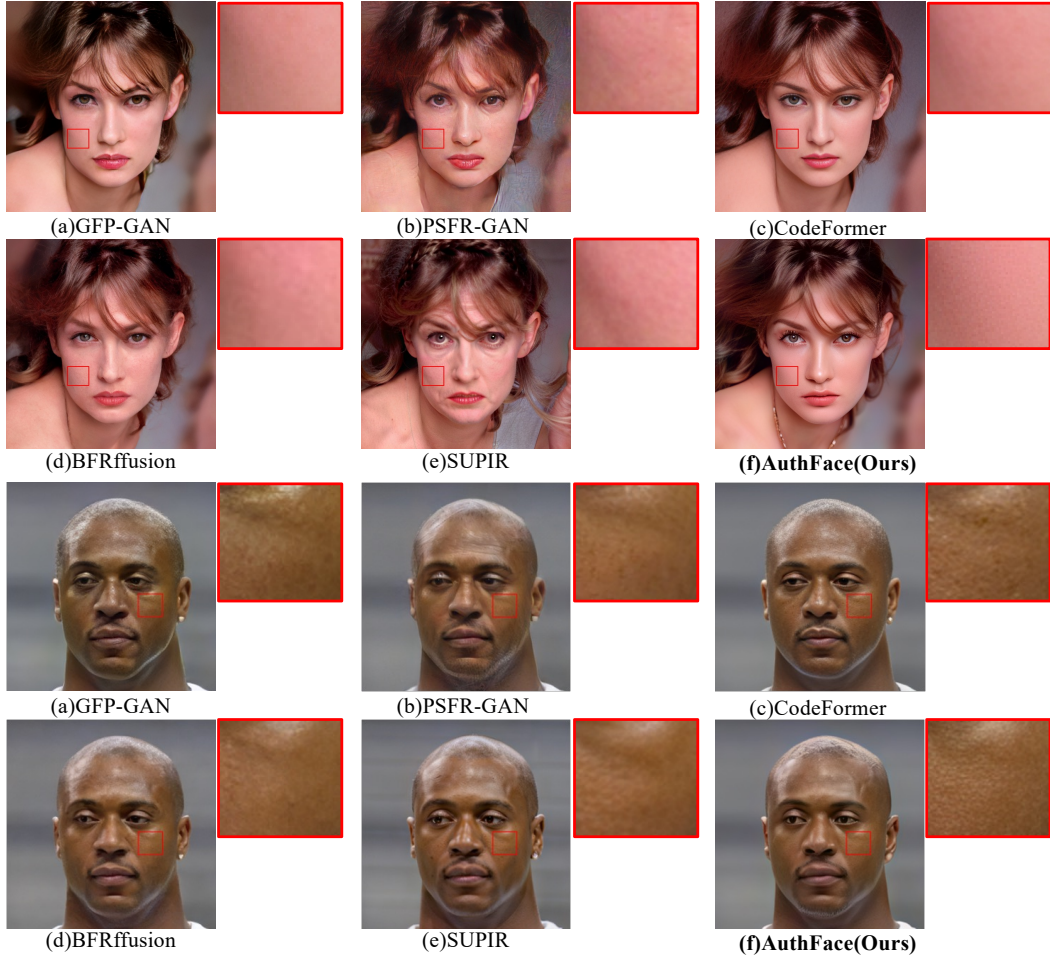


Figure 15: Visualization results in CelebA-Test and LFW-Test dataset including a zoomed-in view of the skin highlighted in **red box areas**. Zoom in for more details.

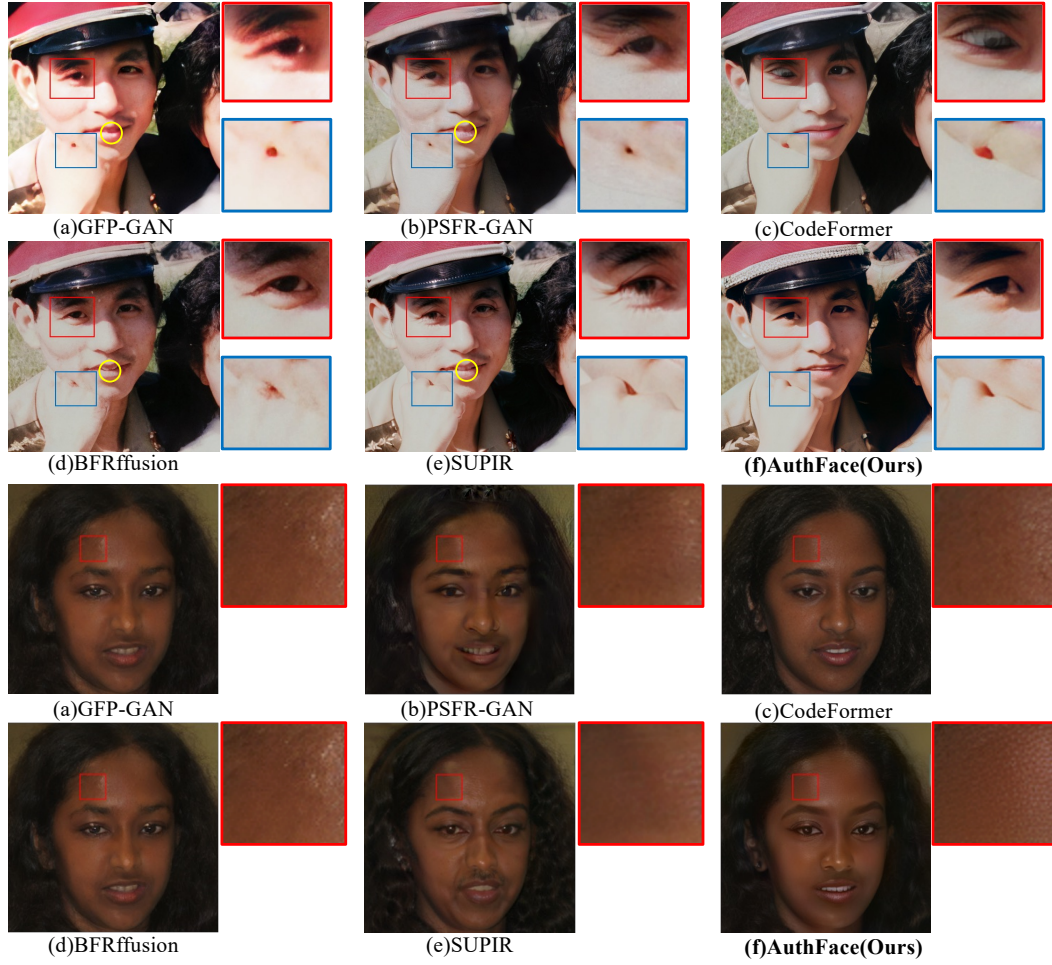


Figure 16: Visualization results in WebPhoto-Test and WIDER-Test dataset. Results in WIDER-Test dataset (2nd case) include a zoomed-in view of the skin highlighted in red box areas. Zoom in for more details.